

Peculiarities of boron distribution in as-grown boron-doped diamond

This content has been downloaded from IOPscience. Please scroll down to see the full text.

2014 Mater. Res. Express 1 035905

(<http://iopscience.iop.org/2053-1591/1/3/035905>)

View [the table of contents for this issue](#), or go to the [journal homepage](#) for more

Download details:

IP Address: 91.235.244.253

This content was downloaded on 04/11/2014 at 20:39

Please note that [terms and conditions apply](#).

Peculiarities of boron distribution in as-grown boron-doped diamond

V D Blank^{1,2}, B A Kulnitskiy^{1,2,4}, I A Perezhogin^{1,2,3}, S A Terentiev¹,
S A Nosukhin¹ and M S Kuznetsov¹

¹ Technological Institute for Superhard and Novel Carbon Materials, Centralnaya str. 7a, Troitsk 142190, Moscow, Russian Federation

² Moscow Institute of Physics and Technology State University, 141700, Institutskiy per. 9, Dolgoprudny, Moscow Region, Russian Federation

³ International Laser Center of M.V. Lomonosov Moscow State University, Russian Federation

E-mail: boris@tisnum.ru

Received 1 August 2014

Accepted for publication 19 August 2014

Published 16 September 2014

Materials Research Express 1 (2014) 035905

doi:[10.1088/2053-1591/1/3/035905](https://doi.org/10.1088/2053-1591/1/3/035905)

Abstract

Boron doped diamond (BDD) single crystals have been grown under conditions of high isostatic pressure by the temperature gradient method. Numerous equilateral triangles were found on the fluorescence images of {111}-diamond facets. Structural peculiarities of BDD were investigated by JEM-2010 transmission electron microscope with GIF Quantum attachment for electron energy loss spectroscopy (EELS). High resolution image of diamond lattice revealed some distorted {111}-layers. EELS testifies the presence of boron in distorted regions of diamond lattice. The crystallographic features of BDD and their connection with the superconductivity are discussed.

Keywords: boron-doped diamond, crystal structure defects, transmission electron microscopy, fluorescence imaging, diffusion

1. Introduction

Owing to its unique physical properties, diamond is a very prospective material for applications in electronic devices working under extreme conditions. Diamond can serve as a heat sink due to its high thermal conductivity, or as an acoustic conductor due to the high value of the speed of sound in it. It has big values of breakdown voltage and operating voltage, high radiation resistance and capability of usage at high temperatures. Diamond is chemically stable, insoluble in acids, very hard, and it has low dielectric permittivity [1–3].

⁴ Author to whom any correspondence should be addressed.

Boron is often used as a doping element in order to alter the properties of a diamond. Boron has one electron fewer than carbon and, because of its small atomic radius, boron is relatively easily incorporated into diamond. Boron creates a deep acceptor energy level with activation energy $E_a = 0.37$ eV. Since boron acts as a charge acceptor, the resulting diamond is effectively hole-doped (*p*-type) semiconductor [4] at low boron concentration ($n \approx 10^{17} \div 10^{19} \text{ cm}^{-3}$), and it can acquire some metal-like properties at $n \geq 10^{20} \text{ cm}^{-3}$. Apart from this, boron is a component of the only high-temperature superconductor MgB_2 possessing the electron–phonon mechanism of electron coupling [5, 6]. Doping of a diamond with boron makes the diamond a superconductor [7], though a low-temperature one ($T_c = 4$ K). In spite of the fact that the doping of a diamond with boron yields new interesting properties and applications of a diamond, the structure of a boron-doped diamond (BDD) is not studied thoroughly. In the present work we aim to analyze in detail the single-crystal BDD structural features.

2. Experimental

The synthesis of the single-crystal boron-doped diamond (BDD) was performed under the conditions of thermodynamic stability of a diamond under high pressure by the temperature gradient method [8, 9]. This method is based on maintaining the temperature difference within the high-pressure growth cell between the origin of the carbon (high-temperature area) and the growing diamond crystal (lower temperature). High purity (99.95%) graphite was used as a carbon source. Boron source was amorphous boron (99% purity) placed in a bulk of carbon source. Fe–Al alloy was used as a crystallization medium [10]. The crystallization temperature was 1880 ± 20 K. The duration of the crystallization periods was 160 ± 5 h. After the crystallization process was finished, the diamond single crystal was taken out of the growth medium. Then a $35\text{--}40 \mu\text{m}$ parallel plate was cut by a laser beam from the (111) facet of the diamond. In order to study the diamond in a transmission electron microscope (TEM), this plate was mechanically broken into small fragments which were placed onto a TEM grid. The TEM studies of the BDD were performed using a JEM-2010 microscope with a GIF Quantum attachment for electron energy loss spectroscopy (EELS). The sample was also studied in a JSM-7600F scanning electron microscope with attachments for energy-dispersive x-ray spectroscopy (EDS) and wavelength-dispersive x-ray spectroscopy (WDS). We obtained some fluorescence images of {111} facets illuminated by ultraviolet radiation (225 nm wavelength) in the DiamondView instrument (The Diamond Trading Company Limited, UK). The depth of the fluorescence excitation in the diamond was about some microns (according to the DiamondView specification).

3. The discussion of results

Figure 1 shows a faceted diamond crystal with a small boron concentration. The amount of boron in a high-pressure chamber during the synthesis was 0.025% of graphite mass. Numerous equilateral triangles are seen at the large upper facet (111). Their sides are parallel to the facets of the diamond. This contrast disappears after polishing. Taking into account the polishing depth for the (111) facet, the thickness of the contrast layer should be approximately 1 micron. The analysis of a number of such crystals has shown that the triangles are seen only in the

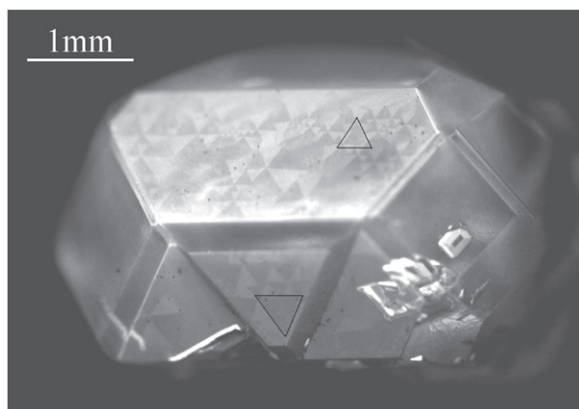


Figure 1. The fluorescence image of the surface layer of (111) diamond facet illuminated by ultraviolet. A BDD grown in a crystallization medium with boron content 0.3 mg. {111} facets of diamond are separated by $\langle 110 \rangle$ directions. Numerous equilateral triangles are seen which sides are parallel to the facets of diamond.

{111} planes, and the lines separating these triangles coincide with the $\langle 110 \rangle$ directions in the diamond lattice. Therefore, the crystallographic analysis of figure 1 shows that the surface layer having a $1 \mu\text{m}$ thickness yields the contrast seen as the triangles separated by the {111} planes intersecting the (111) facet at the $\langle 110 \rangle$ directions (parallel to the triangle sides). The WDS analysis in a scanning electron microscope has shown that the dark triangles contain more boron than the light ones. It can be seen from figure 1 that the $(11\bar{1})$ facet neighboring the upper (111) facet also shows a triangular contrast (two triangles on these two facets are marked by black contours in the figure). At that, the bases of the triangles at both facets are parallel to the line separating these facets. An increase in the boron concentration leads to the appearance of the isosceles triangles along with the equilateral ones, where the apex angle is different from 60° . Sometimes the sides of the triangles are not straight but rather are composed of straight segments which constitute slightly different angles with the base of the triangle. In certain cases we observed similar triangles but of a much bigger size at the (111) surface of the diamond. Origination of such structures takes place if the cooling begins from higher temperatures (higher than the metal catalyst melting temperature) and proceeds slower. It is known that slow and fast quenching corresponds to a different amount of surface crystallization seeds. In the case of slow quenching, the amount of triangles is smaller, but the triangles themselves are bigger.

In order to explain the appearance of the triangular contrast, it is necessary to take into account the growth processes accompanied by the boron diffusion (figure 2). Diffusion is a process which is activated thermally. Under the conditions of our experiment, a thermal diffusion takes place, which is the diffusion caused by the temperature gradient dT/dx . Apart from this, an ascending diffusion may take place, i.e., the diffusion caused by the gradient of elastic strain and stress dU/dx . If the crystal under pressure is heated, then it tends to minimize the elastic strain and stress which activates the diffusion.

In a diamond, the closely packed layers ABCABC... are perpendicular to the $\langle 111 \rangle$ directions. All the planes {111} and the directions $\langle 110 \rangle$ belonging to them are most closely packed planes and directions in a crystal. Unlike a hexagonal closely packed (HCP) lattice with ABAB... stacking, which has empty channels in it favoring the diffusion, there are no such

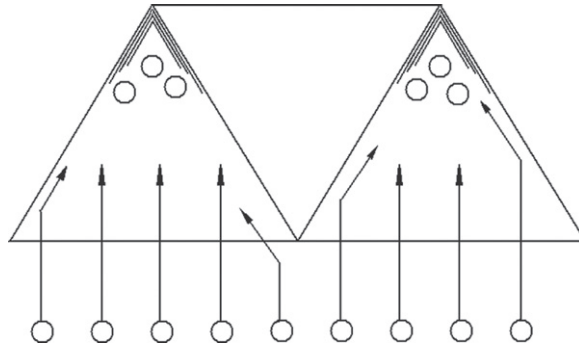


Figure 2. Proposed scheme of boron diffusion in diamond. At the first stage the $\{111\}$ planes saturate with boron atoms, and then the boron atoms diffuse along $\{111\}$ planes and accumulate near the apex of the triangle, changing the contrast. At that, the triangle becomes isosceles instead of being equilateral. Boron atoms do not penetrate into oppositely oriented triangles, since the atoms bypass them.

channels in the diamond lattice. Therefore, even though a boron atom radius is less than a carbon atom radius, the diamond lattice structure obstructs the diffusion of boron.

Nevertheless, the boron atoms move inside the diamond at high temperatures from regions with a higher temperature to those with a lower one. They get stuck in most closely packed layers $\{111\}$ of diamond, at a distance where they completely lose their energy. The diffusion of alien atoms in a single crystal is always anisotropic, and there can exist more favorable and less favorable directions for the diffusion. We did not encounter any evidences in the scientific literature for diamond on the diffusion rates in different crystallographic directions, but to all appearances, the diffusion in the $[111]$ direction should be most blocked. The only experimentally established fact is that the diffusion rate is lowest perpendicularly to the $\{111\}$ plane in a semiconducting composition lattice of a diamond-type during the ion implantation [11]. As in our work, alien atoms possessing kinetic energy penetrate into the diamond-like structure.

However, we do not have any explanation on the way the boron atoms remain in the $\{111\}$ diamond planes. Regardless, the $\{111\}$ planes distortion occurs. This is testified by the fact that in the case of cooling from higher temperatures, the size of the triangles is bigger. This can be due to higher kinetic energy of the boron atoms, which allows them to penetrate at longer distances. Then the sides of the triangles are formed (boron atoms reach the intersection with another $\{111\}$ plane), the new coming boron atoms will reach the lateral sides of the triangles, and move along them (since they cannot penetrate through them) to the triangle apex. As a result, they deposit mostly in those fragments of the $\{111\}$ planes which are located close to the apex. It changes the angles of the triangles. Boron atoms penetrate into the triangles perpendicularly to the triangle base, so, the boron concentration in such triangles is higher. At the same time, the triangles with apexes oriented in the opposite way do not contain boron, since boron atoms bypass these apexes at right and left sides, as is shown in the figure 2, penetrating into the neighboring triangles. The same mechanism is realized on the top facet. Boron atoms penetrate into the triangles only through the base and not through the apex.

We have studied the pieces of the surface layer of the sample in a TEM. EELS was used in order to detect the boron atoms. We observed (separately) two distinct features of the presence of boron in the sample. Figures 3 and 4 show the first one, namely, the fragments containing the

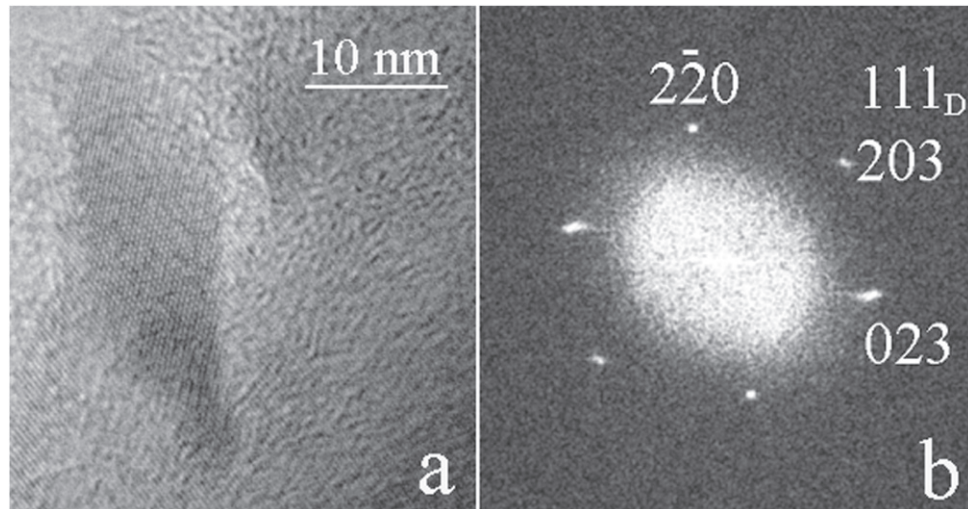


Figure 3. (a) The boron carbide fragment at the surface of the diamond. The crystal lattice of B_4C is clearly seen. (c) the diffraction pattern taken from (a); from (a) it follows that $(203)_{B_4C} \parallel (111)_D$.

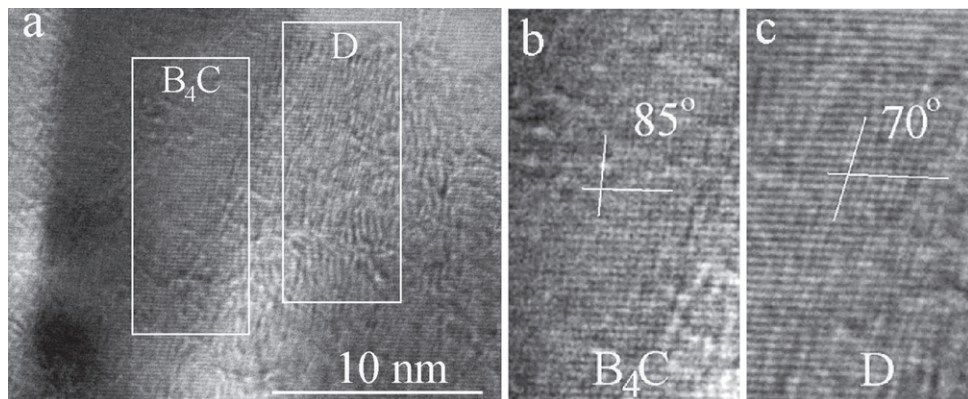


Figure 4. (a) The boron carbide fragment at the surface of the diamond. (b), (c) The high resolution images of the fragments shown in white rectangles in (a); (b)—boron carbide (B_4C) lattice; (c)—diamond lattice. Their zone axes are $[120]_{B_4C}$ and $[110]_D$ correspondingly. Planes $(2\bar{1}4)$ and $(2\bar{1}\bar{4})$ of boron carbide composing 85° -angle are indicated by white lines in (b). (111) and $(11\bar{1})$ of diamond composing 70° are indicated in the same way in (c). $(2\bar{1}4)_{B_4C} \parallel (111)_D$.

boron carbide. Figure 3(a) shows a particle of the boron carbide on the surface of the diamond. Figure 3(b) shows the corresponding diffraction patterns. The reciprocal lattice section seen in it fits the section of B_4C hexagonal lattice, where $a=0.56$ nm, $c=1.207$ nm [12]. It follows from the image that $(203)_{B_4C} \parallel (111)_D$. Figure 4(a) shows another boron carbide particle on the diamond surface. Figures 4(b), (c) show the high-resolution images fragments taken in rectangles in figure 4(a). The zone axis of the boron carbide in figure 4(b) is $[120]_{B_4C}$ (here ‘ B_4C ’ sub-index stands for the boron carbide), and the zone axis of the diamond in figure 4(c) is $[110]_D$ (sub-‘D’ stands for the diamond). The atomic planes $(2\bar{1}4)$ and $(2\bar{1}\bar{4})$ of boron carbide are indicated in figure 4(b), and the angle between them is approximately equal to 85° . Planes

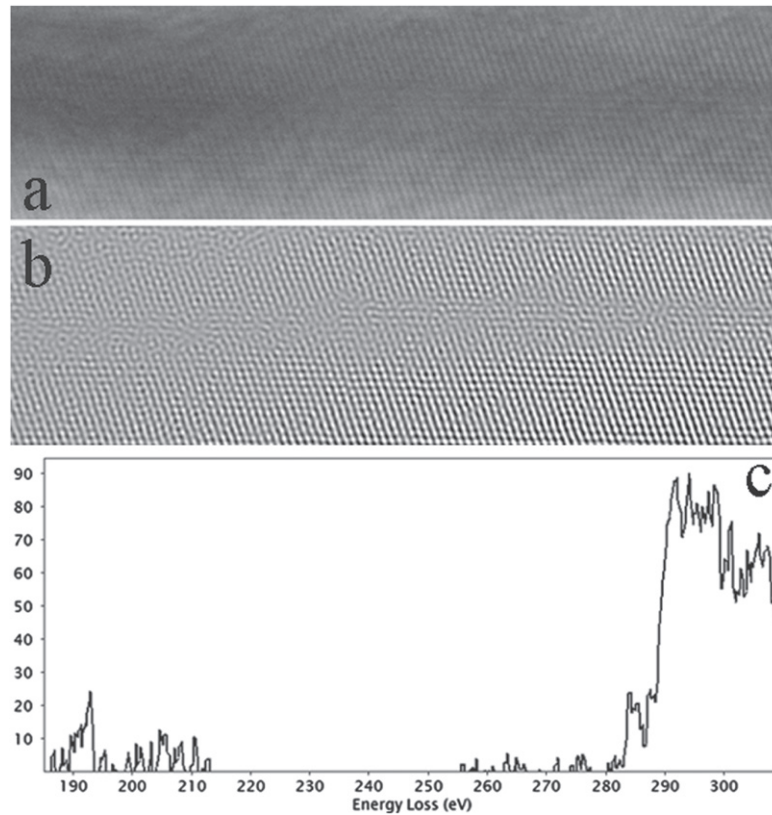


Figure 5. (a) High resolution image of the diamond lattice. The zone axis is [110]. There are some irregularity of the lattice ($\{111\}$ planes) and change in contrast in the horizontal band in the middle of the image. (b) Fourier-filtered image (a). (c) EELS spectrum showing the presence of weak signal near boron K-edge (188 eV) and strong signal at carbon K-edge (284 eV).

(111) and $(11\bar{1})$ of the diamond compose an angle of (approximately) 70° . At that, $(2\bar{1}4)_{B_4C} \parallel (111)_D$.

The second feature indicating the presence of boron is shown in figure 5. A high-resolution image of the diamond lattice is shown. In the central part of figure 5(a), a horizontal band is seen consisting of several (111) atomic layers with some distortion of its structure. The Fourier-filtered image is shown in figure 5(b). The distortion is local, and there are no extensive defects like twinning or stacking faults. The EELS analysis (figure 5(c)) testifies to the presence of boron in this area. The spectra acquired from other regions which do not contain any defect layers show no signal at the position of the boron K-edge. Therefore, we believe that the distortion in the lattice is caused by the presence of boron atoms which accumulate in some $\{111\}$ layers of the diamond.

It should be taken into account that the diamond crystal surface formation can proceed also after its growth ceases. At this moment, it can be considered as quenching, since the cooling rate achieves hundreds of degrees per minute. In order to consider the formation of the surface structure, it is necessary to take into account two main issues: a) a high concentration of vacancies in the vicinity of the growing crystal facet [13]; b) the content of boron at the boundary between the liquid and the crystal. Both these conditions act simultaneously and

affect the formation of the crystal surface structure. Nevertheless, let us consider these issues separately. First, the vacancy mechanism of the defect structure formation in the surface. When the external heating stops, the growth of the diamond still proceeds but under other kinetic conditions; for this case, we assume that the pressure is constant and that the temperature field changes rapidly. The post-growth of the diamond surface will proceed until the temperature falls below the critical temperature (in accordance with the P-T diagram). In our case, this temperature will be lower compared to that of a single-component system, because the boron concentration in the liquid is much higher than in the crystal [13]. The growing surface layer of the diamond will have high concentration of vacancies. Simultaneously, the flow of vacancies moving to the surface of the crystal will capture and carry the boron atoms, which will lead to the boron concentration growth. Further lowering of the temperature will be accompanied by the condensation of the vacancies in the {111} plane. This phenomenon is well known in many of the quenched face-centered cubic (FCC) crystals with low energy of the stacking fault. It can be described by the model proposed by Christian [14]. A flat vacancy disk collapses and yields the triangle-shaped loop of a Frank dislocation with sides parallel to the directions $\langle 110 \rangle$ in the plane {111}. For a diamond, the energy of formation of such a defect is low, and there occurs a decrease in the elastic energy by means of the stacking fault area growth. Further, the Frank dislocation parallel to the closely packed direction dissociates into the stair-rod dislocation and Shockley dislocation. As a result of further dislocation reactions [14] of the following type

$$\frac{a}{3}[111] = \frac{a}{6}[101] + \frac{a}{6}[121] \quad (1)$$

there originates a tetrahedron composed of stacking faults, the edges of which are the stair-rod dislocations. There are also other collapse mechanisms of the 3D-clusters of vacancies, but the result of any of them is the formation of tetrahedra in the FCC structures. In this mechanism (dissociation of Frank dislocation and formation of tetrahedra), the relaxation of the elastic stress realizes not only through the dislocation reactions, but also by means of promoted boron diffusion to the extra-planes of the edge dislocations, which leads to a decrease in the diamond lattice deformation due to the concentration lowering in the defect-free area. Simultaneously, when the boron concentration becomes high enough and the boron carbide formation takes place, then strict orientation relationship between the boron carbide lattice and the diamond lattice should be satisfied.

At the same time, the residual growth of the diamond surface still proceeds, and another mechanism of elastic stress relaxation is possible, which is caused by the high boron concentration. Estimating the elastic stress influence on the diamond growth shows that the doping element concentration cannot exceed 0.001 atomic %. Otherwise it will result in a high rate of internal energy growth, which, in its turn, should not exceed the theoretical toughness of the crystal $E_0(c) < \tau^2/2\mu$, where τ is the value of elastic stress. Therefore, such a concentration inevitably results in inability of a crystal growth under the given P-T conditions. From [15] it is known that

$$E_0(c) = 4\mu\varepsilon^2\Omega Nc(1 - c) \quad (2)$$

where E_0 is the internal energy of the system, c is the concentration of the doping element (boron), μ is a shear modulus (of a diamond), ε is the elastic stress of a lattice, Ω is a mean atom volume, N is the number of atoms. Therefore, it is necessary to provide the relaxation of the elastic stress caused by the difference of the atomic radii of boron and carbon. It is necessary to

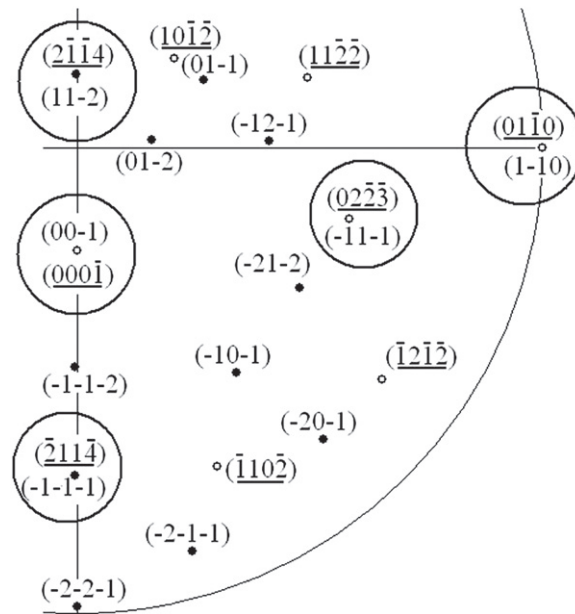


Figure 6. The fragment of the combined stereoprojection of boron carbide and diamond, plotted in accordance with their mutual orientation observed experimentally.

remark that the crystal growth proceeds at a temperature which is reasonably lower than the Debye temperature, i.e. $T_{\text{growth}} \approx 1800 \text{ K} < 2160 \text{ K} = T_{\theta}$, therefore, it can be treated as a low-temperature one. Such a situation is natural for the martensitic transformations, where the elastic stress plays the most important role. In this case, the crystal growth proceeds through the formation of flat disks or plates, the value of elastic stress which depends on the h/R ratio, where h is a thickness of a disk (a plate) and R is its radius (transversal size) [14], i.e., the thinner a plate is, the better is the relaxation. The collapse of the vacancy disks (with higher boron concentration) accompanied by the formation of the stacking faults can result (in a limit) in the formation of two atomic layers of boron inside the system of the (111) diamond planes. Therefore, it is direct analogue of the martensitic plate providing almost complete relaxation of an elastic stress in a growing layer of the crystal. This very mechanism of the diamond surface growth can provide a high growth rate and yield a layered structure observed in the HRTEM.

We analyzed the obtained diffraction patterns and plotted a combined stereoprojection (SP) of the diamond and boron carbide B_4C . The fragment of this SP is shown in figure 6. It follows from this fragment, that the $\{111\}$ of the diamond coincides with the $(02\bar{2}\bar{3})$ and $(\bar{2}11\bar{4})$ of boron carbide with good precision. The circles in the figure mark the SP fragments where the crystallographic planes of diamond and boron carbide are shown, the parallelism of which was observed experimentally. It also follows from the SP that the $(01\bar{1}0)_{B_4C}$ coincides with the $(1\bar{1}0)_D$. The orientation relationship between the crystal lattices of diamond and boron carbide is the following:

$$\begin{aligned} (1\bar{1}0)_{\text{diam}} &\parallel (01\bar{1}0)_{B_4C} \\ [001]_{\text{diam}} &\parallel [0001]_{B_4C}. \end{aligned} \quad (3)$$

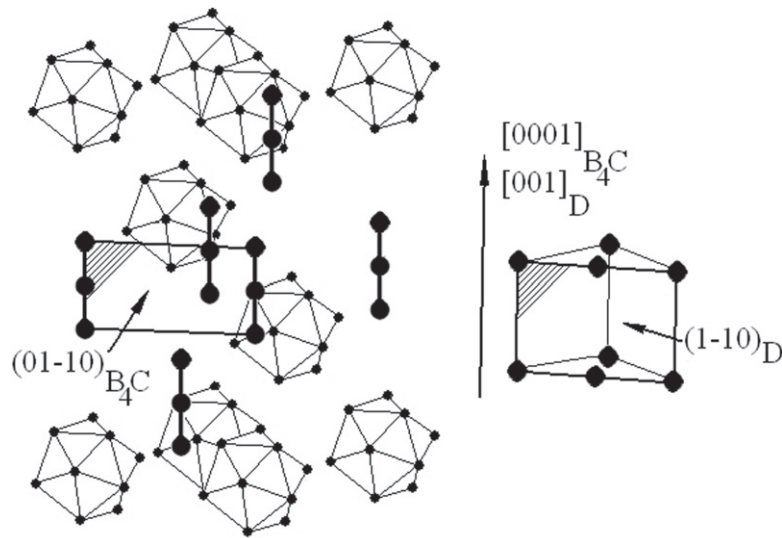


Figure 7. The schematic images of the lattices of boron carbide (left) and diamond (right). (Only certain atoms are shown in diamond lattice in order not to overload a scheme). The boron atoms (small black circles) compose dodecagons, which are located in the corners of the B_4C elementary unit cell. Carbon atoms are shown as larger black circles. Planes $(01\bar{1}0)_{B_4C}$ and $(1\bar{1}0)_D$ are parallel in accordance with the experimentally observed orientation relationship. In this scheme they are marked by partial shading.

The lattice of the single-crystal fragments containing boron shown in figures 3 and 4 were identified as B_4C . Actually, in the TEM it is very difficult to distinguish between the known up to the present time B_4C and $B_{13}C_2$, since their lattices have very close lattice parameters. Thus, for B_4C $a=0.560$ nm, $c=1.208$ nm, whereas for $B_{13}C_2$ $a=0.563$ nm and $c=1.216$ nm. B_4C contains icosahedra consisting of 12 boron atoms and a C-C-C chain (figure 7). And if one of the carbon atoms in this chain is replaced by the boron atom, the chain becomes the following C-B-C [16]. For $B_{13}C_2$, the chains will be C-B-C and C-B-B [16]. The length of the bonds in different chains will be different. Figure 7 shows a crystal lattice of boron carbide B_4C [17] and diamond oriented in accordance with (3). The fragment of the lattice (shown as a rectangle) containing three carbon atoms (or, probably, one or two of them are substituted by the boron atoms) has a size of approximately 0.3 nm along the [001] direction and 0.56 nm in the perpendicular direction, whereas the corresponding distances in the (110) plane of a diamond are 0.356 nm and 0.503 nm. So, during the boron carbide formation from the diamond, the rearrangement of the atoms and a lattice deformation have taken place.

As was mentioned above, the investigations of BDD are in close connection with the superconductivity observed in such crystals. The superconductivity was observed in the surface layer of a BDD. It was noted [18] that the boron content in diamond CVD films decreased significantly after the surface polish. In the same work it was shown that after polishing, the diamond conductivity lowered. It was shown that boron content decreased gradually in the depth of the surface [19]. The modulation of superconducting properties of a heavily boron-doped diamond by tuning the surface electronic state was shown in [20]. We suppose that in our case the superconductivity can appear due to the disorder of structure in the diamond lattice layers saturated with boron (figure 5). Indeed, in [21] it was shown that the disorder plays a key

role in the electronic structure and affects the critical temperature (T_c) of superconductivity of the BDD.

Calculation [22] of the band structure of the BDD combined with the assumption of a Bardeen–Cooper–Schrieffer (BCS) type pairing mechanism [23], allow one to suggest that superconductivity arises from the coupling of phonons with holes at the top of σ -bonding (valence) bands, in a way similar to MgB_2 [5, 6]. Both the contraction of the reconstructed bonds and the 2D nature of the surface states may exist in the BDD surface, they can also induce a stronger electron–phonon coupling and lead to the larger value of the T_c [24]. Recently [25, 26, 21] have calculated the dependence of T_c on the disorderly nature of boron in the superconducting BDD. According to their results, a boron ion disorder induces the broadening of the density of states at Fermi level, as well as the very short life time and mean free path due to the large imaginary part of the self-energy. A micrometer-sized grain is separated from other grains by a clearly visible straight boron-rich boundary.

Since a BDD contains inclusions of boron carbide as well, one should carefully consider their role in superconducting behavior. The possibility of making superconducting materials based on the boron carbide family is being explored [27], but so far it does not have any results. In [28] the IR spectroscopy of boron carbide has shown its semiconductive behavior. No evidences for the superconductivity were observed. At the same time, the possible occurrence of superconductivity from hole doping boron icosahedra was studied in [29]. The possibility of having high superconducting T_c in these systems was found. As a possible physical realization of a metallic state $B_{13}C_2$ was considered, which is formed from B_{12} icosahedral units with one hole per icosahedron. Using *ab initio* calculations, the authors have determined its normal state properties, finding a moderate electron–phonon coupling and a large phonon logarithmic average to the phonon frequencies. It was demonstrated that both properties are connected to the B_{12} building blocks. Indeed, the local density of state at the Fermi level and the phonon modes strongly coupled with electrons are localized on the icosahedra. Therefore, the presence of boron carbide can also be considered as an origin of the superconductivity of a BDD.

4. Conclusion

BDDs are grown by a temperature gradient method. It has been established that the boron accumulates in a surface layer of the (111) facet of a diamond in an approximately $1\ \mu\text{m}$ thick layer. The fluorescence view of the surface shows numerous equilateral triangles, which become not equilateral (angles change) with the growth of boron amount in the BDD. The introduction of boron atoms in a diamond yields two effects: the disorder of the {111} planes of diamond and the boron carbide formation. We believe that the superconductivity in a BDD observed earlier appears due to one of the two above-mentioned features. We have established the orientation relationship between the diamond lattice and the B_4C lattice. It is shown that in the surface layer of the diamond lattice there appear some defect layers consisting of several (111) planes distorted by boron atoms.

Acknowledgements

This work was supported by the Ministry of Education and Science of Russian Federation within the framework of State Contract 14.577.21.0090.

References

- [1] Field J E 1992 *The Properties of Natural and Synthetic Diamond* (New York: Academic) p 710
- [2] Prelas M A, Popovici G and Bigelow L K 1998 *Handbook of Industrial Diamonds and Diamond Films* (New York: Marcel Dekker Inc.) p 1179
- [3] Nazare H A and Neves J 2001 *Properties, Growth and Applications of Diamond* (London: INSPEC) p 431
- [4] Wang Z L *et al* 2006 The superconductivity in boron-doped polycrystalline diamond thick films *Diam. Rel. Mat.* **15** 659–63
- [5] Nagamatsu J, Nakagawa N, Muranaka T, Zenitani Y and Akimitsu J 2001 Superconductivity at 39 K in magnesium diboride *Nature* **410** 63–4
- [6] Kortus J, Mazin I I, Belashenko K D, Antropov V P and Boyer L L 2001 Superconductivity of metallic boron in MgB₂ *Phys. Rev. Lett.* **86** 4656–9
- [7] Ekimov E A, Sidorov V A, Bauer E D, Mel'nik N N, Curro N J, Thompson J D and Stishov S M 2004 Superconductivity in diamond *Nature* **428** 542–5
- [8] Wentorf R H Jr 1971 Diamond growth rates *J. Phys. Chem.* **75** 1833–7
- [9] Strong H M and Chrenko R M 1971 Diamond growth rates and physical properties of laboratory-made diamond *J. Phys. Chem.* **75** 1838–43
- [10] Blank V D, Kuznetsov M S, Nosukhin S A, Terentiev S A and Denisov V N 2007 The influence of crystallization temperature and boron concentration in growth environment on its distribution in growth sectors of type IIb diamond *Diam. Rel. Mat.* **16** 800–4
- [11] Thevenot F 1990 Boron carbide—a comprehensive review *J. Eur. Ceram. Soc.* **6** 205–25
- [12] Titov V V 1986 Defects formation under channeling surface (Russian) *Phys. Chem. Mech.* **11** 908
- [13] Lyubov B Y 1969 *The Kinetic Theory of Phase Transitions* (Moscow: Metallurgiya) p 264
- [14] Christian J W 1965 *Theory of Transformations in Metals and Alloys* (Oxford: Pergamon Press) p 1200
- [15] Goldsmid H J 1973 *Problems in Solid State Physics* (London: Pion limited) p 483
- [16] Emin D 1988 Structure and single-phase regime of boron carbides *Phys. Rev. B* **38** 6041–55
- [17] Domnich V, Reynaud S, Haber R A and Chhowalla M 2011 Boron carbide: structure, properties, and stability under stress *J. Am. Ceram. Soc.* **94** 3605–28
- [18] Wu D, Ma Y I, Wang Z L, Luo Q, Gu C Z, Wang N L, Li C Y, Lu X Y and Jin Z S 2006 Optical properties of boron-doped diamond *Phys. Rev. B* **73** 012501
- [19] Mavrin B N, Denisov V N, Popova D M, Skryleva E A, Kuznetsov M S, Nosukhin S A, Terentiev S A and Blank V D 2008 Boron distribution in the subsurface region of heavily doped IIb type diamond *Phys. Lett. A* **372** 3914–8
- [20] Natsui K, Yamamoto T, Watanabe T and Einaga Y 2012 Influence of surface termination of boron-doped diamond on superconducting property *American Physical Society APS Meeting* abstract #W21.008
- [21] Ohta Y 2007 Theoretical aspects of superconductivity in boron-doped diamond *New. Diam. Front. C. Tec.* **17** 33–44
- [22] Bustarret E, Achatz P, Sacépé B, Chapelier C, Marcenat C, Ortéga L and Klein T 2008 Metal-to-insulator transition and superconductivity in boron-doped diamond *Phil. Trans. R. Soc. A* **366** 267–79
- [23] Bardeen J, Cooper L N and Schrieffer J R 1957 Theory of superconductivity *Phys. Rev.* **108** 1175
- [24] Wang Z L *et al* 2006 The superconductivity in boron-doped polycrystalline diamond thick films *Diam. Rel. Mater.* **15** 659–63
- [25] Kato Y, Matsui F, Shimizu T, Daimon H, Matsushita T, Guo F Z and Tsuno T 2007 Dopant-site effect in superconducting diamond (111) studied by atomic stereography *Appl. Phys. Lett.* **91** 251914
- [26] Shirakawa T, Horiuchi S, Ohta Y and Fukuyama H 2007 Theoretical study on superconductivity in boron-doped diamond *J. Phys. Soc. JPN* **76** 01471120
- [27] Balakrishnarajan M M, Pancharatna P D and Hoffman R 2007 Structure and bonding in boron carbide: the invincibility of imperfections *New J. Chem.* **31** 473–85

- [28] Werheit H and Kuhlman U 2011 Superconductivity in boron carbide? clarification by low-temperature MIR/FIR spectra *J. Phys.-Condens. Matt.* **23** 435501
- [29] Calandra M, Vast N and Mauri F 2004 Superconductivity from doping boron icosahedra *Phys. Rev. B* **69** 224505–10